Study on bearing performance for inching worm locomotion using characteristics of wheel subsidence on loose soil

Daisuke Fujiwara[1] and Kojiro Iizuka[2]

Abstract— **In general, slipping and sinking on the rough terrain is lead to poor condition for planetary explorations robot, which is equipped with a cylindrical typed wheel. Meanwhile, in a robot, which is equipped with inching worm locomotion, slipping and sinking lead to increase a traveling performance because the more sinking and slipping of the robot is, the larger the bearing force in the back of a wheel increases. Moreover, in the inching locomotion, the wheel travels during sharing soil beneath the wheel and pushing soil in backward. However, this model was not investigated before. This paper investigates the relationship between the bearing force in the back of the wheel and sinkage. For analysis, firstly, this paper performs theoretical consideration and numerical simulation of a bearing force using bulldozing resistance model. Secondly, this paper performs wheel bulldozing experiment. In order to investigate the difference of bearing force when the wheel size is changed, this paper sets three wheel size. From the simulation and experimental results, the Hegedus's model corresponds with the experimental results in each wheel size. Additionally, the bearing force was observed to increase when the sinkage was increased. Thus, the ability of the inching locomotion using deep sinkage is high.**

I. INTRODUCTION

These days, many studies have been conducted into planetary exploration to the Moon or the Mars. The NASA Mars mission in 1997 launched the rover Sojourner toward the Mars [1]. In 2003, NASA/JPL sent Mars Exploration Rover (MER) toward the Mars [2]. These rovers transmitted important scientific data back to the Earth. The purposes of the planetary exploration are to gather precise information and to investigate a wide range of rocks, soils and clues to past water activity on the planet [3], [4].

However, the Lunar or Martian surface contains loose soil and many steep slopes are located along the crater rims. Therefore, while traversing the loose soil, such rovers may easily slip and reach a poor condition. Also, the rovers fail to move forward or backward in order to escape from the poor condition. For example, the MER was sinking into the soil and failed to move forward or backward in 2009. These rovers are required to traverse on the loose soil with slopes $25-30°$. Therefore, the rovers are required high traveling performance to traverse the loose soil [4].

[1]Daisuke Fujiwara is with the Department of Functional Control Systems, Graduate School of Engineering and Science, Shibaura Institute of Technology, 307, Fukasaku, Minuma-ku, Saitama-shi, Japan nb16107@shibaura-it.ac.jp

[2]Kojiro Iizuka is with the Department of Machinery & Control Systems, Colledge of Systems Engineering and Science, Shibaura Institute of Technology, 307, Fukasaku, Minuma-ku, Saitama-shi, Japan iizuka@shibaura-it.ac.jp

To avoid these problems, some previous studies have investigated about a wheeled walking method [5], [6] or an inching worm locomotion method to traverse the loose soil [7]–[12].

A wheeled walking robot ATHLETE, which uses wheels on legs [5], [6], has high traveling performance because it can uses thrust force beneath the wheel. However, the ATHLETE uses a lot of actuators and the system of it is a little bit complex.

Meanwhile, in the inching worm locomotion, Moreland, S. et al. [7] used Scarab rover and analyzed its traveling performance by using drawbar pull index and also analyzed a soil motion beneath the wheel and described the difference of its motion between the rolling wheel mode and inching locomotion mode [8]. Moreover, Creager, C. et al. [9] analyzed traveling performance by measuring a metric travel reduction and a drawbar load of the total rover. From experimental results, the inching worm locomotion indicated high traveling performance and could generate large drawbar pull force in comparison with a conventional rolling mode.

Moreover, Patel, N. et al. and Bauer, R. et al. [10], [11] used ExoMars rover and described the benefit of the inching like locomotion. Kemurdjian, A. et al., [12] developed Marsokhod rover, which has worm-like scheme, and this allows high traveling capabilities.

These inching worm locomotions are a method that utilizes bearing force, which is active between a ground and beneath a wheel. Fig. 1 shows the schematic view of a rolling mode and an inching worm locomotion mode of four wheel rover. From Fig. 1, when the rover operates with the rolling mode, the rover produces thrust by rotating wheel. Meanwhile, when the rover operates with inching worm mode, the rover produces bearing force by keeping a position of a locked wheel relative to a ground. The locked wheel in contact with loose soil push or pull the other rotating wheel using the bearing force. The bearing force of the locked wheel is a sum of a soil pressure, a share stress and other forces from the ground.

When a wheel rotates on loose soil, the wheel sinks into the sand and the bearing surface is generated. In general, the more a wheel sinks, the larger bearing force a wheel generates [13]. However, a static sinkage was used to obtain the bearing force in previous studies [7]–[12]. In our research group, we proposed an advanced scheme that uses a large sinkage to generate the large bearing force and confirmed that that rover had high traveling performance [14]. However, in the previous and our studies, the bearing force of backward wheel didn't discuss enough.

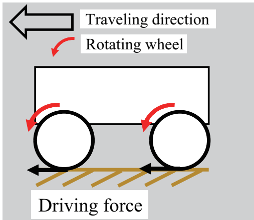

(a) Rolling mode.

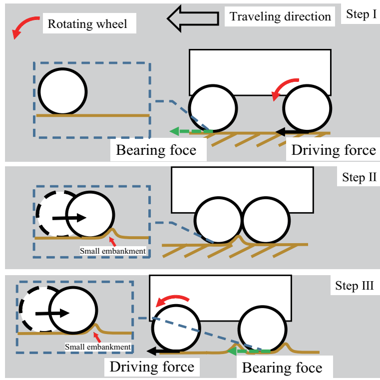

(b) Inching locomotion mode.

Fig. 1: Schematic view of traveling methods.

This paper, firstly, attempts to discuss the bearing force of backward wheel theoretically and calculated the bearing force. Secondly, the bearing force of backward wheel is measured by bulldozing experiments. In order to validate a simulation model, this paper sets three size wheels. Finally, from making a comparison between simulation and experimental results, the relationship between the bearing force and sinkage is discussed.

II. Inching worm locomotion

A. Conventional inching worm locomotion

As mentioned earlier, the conventional sequence of the inching worm locomotion [7]–[12] as shown in Fig. 1, In the stepI, when the rover travels forward direction, the locked wheel pushes soil beneath a wheel toward backward and an embankment is generated. When the locked wheel with 100% skid moves on sand, a soil wedge formed is generated in front of the wheel. This is confirmed by Wong [15]. In this study, we decide this soil wedge formed as an embankment. In the stepI, an embankment supports the locked wheel and the other wheel can move forward direction. Therefore, an embankment is considered as a bearing surface in the inching worm locomotion method and plays an important role.

B. Inching worm locomotion using deeper sinkage

Fig. 3 shows the motion sequence of the inching worm locomotion using deeper sinkage. In motion 1, the wheel of the rover rotates (Fig. 3b) and can get large bearing force from an embankment. Explanation of the motion sequence as follows:

Motion 0: Static situation on loose soil with slope. (Fig. 3a).

Motion 1: The front wheels rotate. The rear wheels stop. (Fig. 3b).

Motion 2: The wheel-base is shortened. (The rover uses bearing force from the backward of the front wheel then the wheel-base is shortened. When the wheel-base is shortened, the rear wheels rotate). (Fig. 3c).

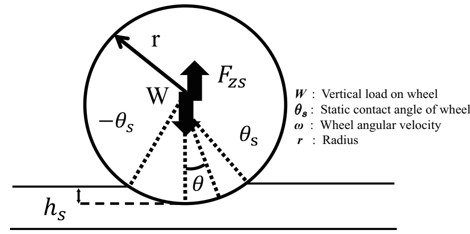

(a) Schematic view of the static sinkage.

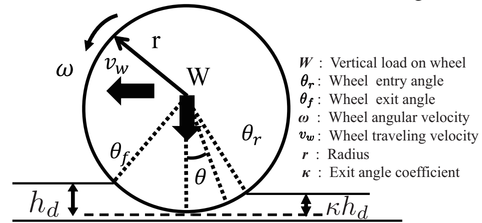

(b) Schematic view of the dynamic sinkage.

Fig. 2: Schematic view of sinkage.

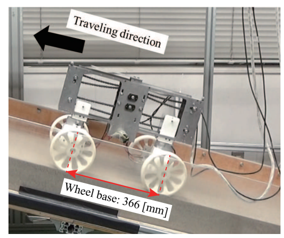

(a) State of motion 0.

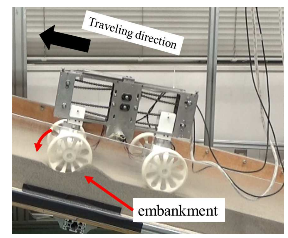

(b) State of motion 1.

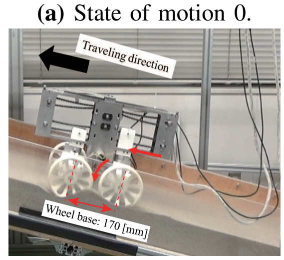

(c) State of motion 2.

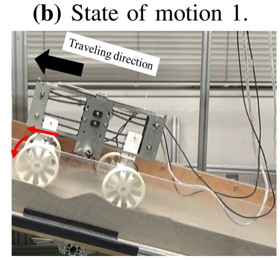

(d) State of motion 3.

Fig. 3: Sequence of the inching worm locomotion using deeper sinkage.

Motion 3: The wheel-base is extended. (When the wheel-base is extended, the front wheels rotate and the rear wheels stop). (Fig. 3d).

III. Mechanism of generating bearing force

A. Wheel sinking

In this section, a wheel sinking mechanics are explained. Interaction mechanics between soil and a wheel has been investigated in *terramechanics* [15]- [18]. When a rover travels on a loose soil, a wheel slips or sinks. In *terramechanics*, a wheel sinkage is defined as static and dynamic. Static sinkage h_s indicates that the sinkage is generated by a normal force of a wheel without a wheel rotation Fig. 2a. Dynamic sinkage h_d indicates that the sinkage is generated by a wheel rotation with arbitrary slip ratios Fig. 2b. Slip ratio is defined by s (1) [15]. Where, v_w is the linear speed of the rover, ω is the angular speed of the wheel, and r is the radius of the wheel.

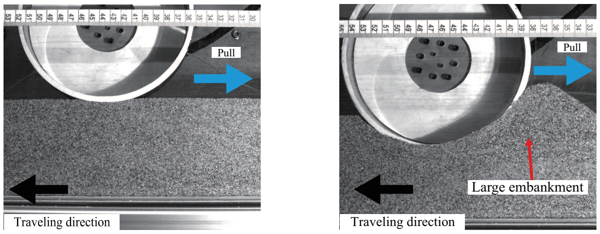

(a) A bearing surface generated by the static sinkage. **(b)** A bearing surface generated by the deep sinkage.

Fig. 4: Wheel is supported by a bearing surface

When the $r\omega$ is larger than v_w, the slip ratio has a value between 0 nad 1. If slip ratio indicates large, the wheel slips and sinks into sand, then, sinkage increases.

$$s = \frac{r\omega - v_w}{r\omega} = 1 - \frac{v_w}{r\omega} \tag{1}$$

Therefore, the sum of the wheel sinkage h_a is showed as follows:

$$h_a = h_s + h_d \tag{2}$$

B. Generateing Bearing surface by wheel sinking

Fig. 4 shows images of sinking wheel and these images are obtained by the high-speed camera. When a wheel puts on loose soil, a wheel sinks into sand as the static sinkage. Meanwhile, when a wheel rotates by large slip ratios, the wheel sinks deeply into sand. When a wheel rotates by small slip ratio, a wheel bulldozes soil in front of a wheel is a dominant phenomenon. Meanwhile, If a wheel rotates by large slip ratio, soil beneath the wheel is transported into backward of the wheel and sinkage becomes deep as shown in Fig. 4b [19]. Therefore, deeper sinkage generates large bearing surface than the static one.

1) Hegedus's bulldozing resistance model: When a locked wheel moves on the loose soil, a locked wheel bulldozes and destroys the soil in front of a wheel. In this situation, a locked wheel receives resistance force from the soil. This resistance force is defined by bulldozing force [18] [20]. In this paper, we assume that bulldozing force is bearing force because the locked wheel gets the bearing force when the wheel supports the inching motion and it bulldozes soil to the back of a wheel.

In order to estimate bearing force of the backward wheel, this study applies Hegedus's bulldozing resistance model [20]. As shown in Fig. 5, when the unit width plate bulldozes soil, the plate pushes the soil to traveling direction and the soil mass is compressed. In this situation, the bulldozing area is defined by a slip surface and a swelled ground. Thus, bulldozing resistance F_p is calculated as follows:

$$F_p(H) = \frac{cot\omega' + tan(\omega' + \phi)}{1 - tan\alpha tan(\omega' + \phi)} \left[H \cdot c + \frac{1}{2}\rho H^2 \times \left\{ (cot\omega' - tan\alpha) + \frac{(cot\omega' - tan\alpha)^2}{tan\alpha + cot\phi} \right\} \right] \tag{3}$$

TABLE I: Parameters of Hegedus model

H	Sinkage	[m]
ω'	Angle between slip surface and ground	[°]
ϕ	International friction angle	[°]
α	Approach angle	[°]
c	Soil cohesion	[-]
ρ	Soil density	[g/cm^3]
b	Plate or wheel width	[m]
F_p	Bulldozing resitance	[N/m]
F	Bulldozing force	[N]

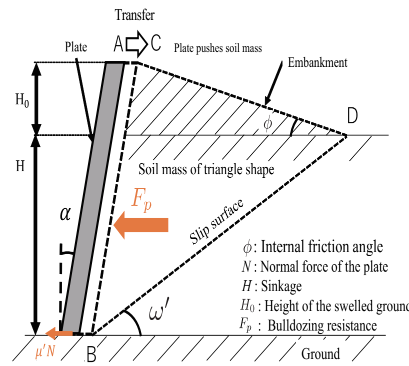

Fig. 5: Bulldozing resistance of hegedus model.

Where, ϕ is an internal friction angle, ω' is an angle between a ground and a slip surface, c is a cohesion of soil, H is a sinkage, ρ is a soil density and α is an approach angle. Table I list each parameter. In this study, ϕ sets an angle of repose. Moreover, based on Coulomb's failure criterion [21], ω' set as follows (4):

$$\omega' = 45° - \frac{\phi}{2} \tag{4}$$

Also, a bulldozing force F of a plate or wheel are obtained as follows (5):

$$F = F_p \times b \tag{5}$$

Where, b is a plate or wheel width. Furthermore, a friction generates beneath a plate $\mu' N$.

From (3), it is confirmed that bulldozing resistance increases depending on increasing sinkage.

2) Bearing surface of the backward wheel: When a locked wheel moves on the soil, a wheel bulldozes soil in front of a wheel and soil swells. The flow pattern and soil wedge formed in front of a wheel are defined by Wong [15] as shown in Fig. 6. According to Wong [15], flow pattern AC is straight. Therefore, in order to estimate a bulldozing force of a wheel, this paper applies Hegedus's bulldozing force and assumes that an approach angle α in Fig. 5 is 0°.

3) Numerical simulation procedure: In order to estimate bulldozing force, the simulations using Hegedus's model performs. The parameters used in the simulation are listed in Table II. According to [22], ρ is determined. According to soil mechanics [21], soil adhesive force of the dry sand is 0, therefore, c is decided as 0. ϕ is equal to the angle of

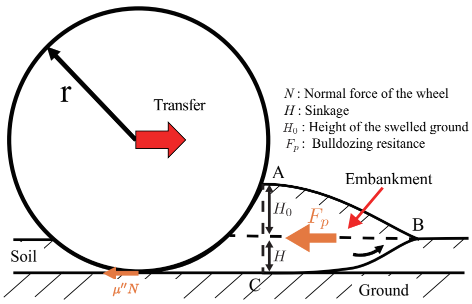

Fig. 6: Bulldozing resistance of wheel model.

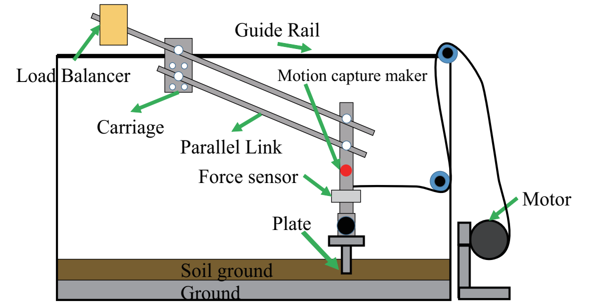

Fig. 7: Schematic view of experimental setting for plate bulldozing test.

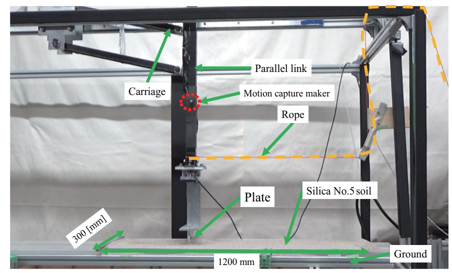

Fig. 8: Overview of experimental setting for plate bulldozing test.

repose and it is experimentally determined. ω' is determined as equation (4), it is based on Coulomb's failure criterion [21].

These parameters input into the equation (3) and calculate the bulldozing resistance. Then, the bulldozing resistance multiplies by a wheel or plate width and calculate bulldozing force.

IV. Experiment

This paper conducts two experiment: 1) A metal plate bulldozing test, and 2) a wheel bulldozing test. These experiments are compared with simulation result respectively. From a metal plate bulldozing experiment and simulation results, validation of Hegedus's model is confirmed in our experiment environment. From a wheel bulldozing experiment and simulation results, the applicability of Hegedus's model for a wheel and relationship between a bearing force and a sinkage is confirmed.

A. Metal plate bulldozing experiment

In order to confirm validation of Hegedus's model, a metal plate bulldozing tests conduct.

1) Experimental environment and conditions: The overview of the experimental system and environment are shown in Fig. 7, 8. The bulldozing area has a width, length and height of 300 $[\mathrm{mm}]$, 1200 $[\mathrm{mm}]$ and $0-30$ $[\mathrm{mm}]$, respectively, and is filled with Silica sand No. 5 as loose soil [22]. The bulldozing force is obtained by force sensor, which sets up upper of the metal plate. The rope, which connects to the pole, pulls the metal plate. The soil specific parameters are listed in Table II.

The metal plate size is 100 $[\mathrm{mm}]$ width, 8 $[\mathrm{mm}]$ length and 70 $[\mathrm{mm}]$ height. The bulldozing speed sets at 36.5 $[\mathrm{mm/s}]$ and sinkage conditions set at $0-30$ $[\mathrm{mm}]$. In sinkage condition of 0 $[\mathrm{mm}]$, the measured force indicates the friction force $\mu' N$ $[\mathrm{N}]$ beneath the plate. The experimental conditions are shown in Table III. Three trials are carried out in each condition.

2) Experimental results: Fig. 9a-9c show the bulldozing force of plate in each sinkage. Fig. 9a-9c show representative results. From every experimental result, the bulldozing force increases as time proceeds and became a steady state. In every result, the friction force, which is active between beneath the plate and soil gound, is eliminated. The friction force is measured from experimental results of sinkage condition 0 $[\mathrm{mm}]$. Also, Fig. 10 shows the relationship between the bulldozing force and the sinkage. In Fig. 10, the continuous line indicates simulation results and the triangle points indicate experimental results of the bulldozing force. The experimental points are the force of the steady state in each experiment and the average value of three trials. From Fig. 10, the force values of the experiment indicate 3.46 $[\mathrm{N}]$ (sinkage 10 $[\mathrm{mm}]$), 8.54 $[\mathrm{N}]$ (sinkage 20 $[\mathrm{mm}]$) and 15.2 $[\mathrm{N}]$ (sinkage 30 $[\mathrm{mm}]$), respectively. Moreover, the difference of the value between the experimental and theoretical value is 1.56 $[\mathrm{N}]$ (sinkage 10 $[\mathrm{mm}]$), 0.95 $[\mathrm{N}]$ (sinkage 20 $[\mathrm{mm}]$) and 1.84 $[\mathrm{N}]$ (sinkage 30 $[\mathrm{mm}]$), respectively. When the sinkage conditions 30 $[\mathrm{mm}]$, we observed that the swelled soil contacted a little to the upper part of the plate. However, this effect relatively small. Therefore, the differences of the value between experiment and simulation result are relatively small. These results confirm that the Hegedus's model is able to represent the bulldozing force of the plate on Silica sand No. 5.

B. Wheel bulldozing experiment

In order to measure bulldozing force of backward wheel, a wheel bulldozing experiments werer conducted in the same way as the experiment of the metal plate.

1) Experimental environment and conditions: The overview of the experimental system and environment are shown in Fig. 11. The bulldozing area and soil are same as the plate bulldozing experiment. The bulldozing force is obtained by force sensor, which set up upper of the wheel. The rope, which connects to the pole, pulls the wheel.

In order to confirm the applicability of Hegedus's model to a wheel, the wheel size is set three sizes. The sizes are 150 $[\mathrm{mm}]$, 170 $[\mathrm{mm}]$ and 200 $[\mathrm{mm}]$ diameter and 40

TABLE II: The soil parameters of Silica sand No. 5 and simulation values

Parameters	Description [Unit]	Value	
		Plate	Wheel
ρ	Soil Dentisy [$\mathrm{g/cm^3}$]	2.60	
c	Soil adhesive force [kPa]	0	
ϕ	Soil internal friction angle [deg]	33	
ω'	Angle between slip surface and ground [°]	$45° - \frac{\phi}{2}$	
b	Width [m]	0.1	0.04
α	Approach angle [°]	0	

TABLE III: Experimental settings for bulldozing plate test.

Slope angle [°]	0
Sinkage [mm]	0, 10, 20, 30
Translational speed [mm/s]	36.5
Soil	Silica sand No. 5
Plate size [mm]	H70 × W100 × D8

$[\mathrm{mm}]$ width. The wheel of 170 mm diameter is the same wheel size of the rover, which equips with advanced scheme (Fig. 3). The bulldozing speed sets at 36.5 $[\mathrm{mm/s}]$ and sinkage conditions set at $0-30$ $[\mathrm{mm}]$. In sinkage condition 0 $[\mathrm{mm}]$, the measured force indicates the friction force $\mu''\mathrm{N}[N]$ beneath the wheel. The experimental conditions are shown in Table IV. Three trials are carried out in each condition.

2) Experimental results: The time history of the bulldozing force in case of wheel experiment shows the same tendency as one of the plates. The time history graph is omitted due to the limitation of the space. Fig. 12 shows the relationship between the sinkage and the bulldozing force in wheel size 170 $[\mathrm{mm}]$. In Fig. 12, the continuous line indicates simulation results and the square points indicates experimental results. The experimental points are the force of the steady state in each experiment and the average value of three trials. In each result, the friction force, which is active between beneath the wheel and soil gound, is eliminated. The friction force is measured from experimental results of sinkage condition 0 $[\mathrm{mm}]$. From Fig. 12, the force values of experiment indicate 1.53 $[\mathrm{N}]$ (sinkage 10 $[\mathrm{mm}]$), 4.29 $[\mathrm{N}]$ (sinkage 20 $[\mathrm{mm}]$) and 7.58 $[\mathrm{N}]$ (sinkage 30 $[\mathrm{mm}]$), respectively. Moreover, the difference of the value betweeen the experimental and theoretical values are 0.86 $[\mathrm{N}]$ (sinkage 10 $[\mathrm{mm}]$), 1.37 $[\mathrm{N}]$ (sinkage 20 $[\mathrm{mm}]$) and 0.72 $[\mathrm{N}]$ (sinkage 30 $[\mathrm{mm}]$), respectively. These difference are relatively small. These results confirm that the Hegedus's model is able to represent the bulldozing force of the plate on Silica sand No. 5.

Moreover, Fig. 13 shows the relationship between the sinkage and the bulldozing force in each wheel size. In Fig. 13, the continuous line indicates simulation results and the circular and the cross mark points indicate experimental results of wheel size 150 $[\mathrm{mm}]$ and 200 $[\mathrm{mm}]$, respectively. The experimental values are the average value of three trials. From Fig. 12, the force values of experiment in wheel size 150 $[\mathrm{mm}]$ indicate 1.49 $[\mathrm{N}]$ (sinkage 10 $[\mathrm{mm}]$), 4.04 $[\mathrm{N}]$ (sinkage 20 $[\mathrm{mm}]$) and 8.29 $[\mathrm{N}]$(sinkage 30 $[\mathrm{mm}]$), respectively. Then, the force values of experiment in wheel size 200 $[\mathrm{mm}]$ indicate 1.46 $[\mathrm{N}]$ (sinkage 10 $[\mathrm{mm}]$), 3.97 $[\mathrm{N}]$ (sinkage 20 $[\mathrm{mm}]$) and 7.49 $[\mathrm{N}]$ (sinkage 30 $[\mathrm{mm}]$), respectively.

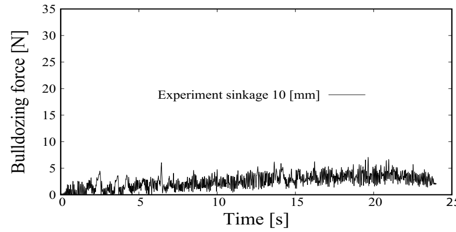

(a) Time history of the bulldozing force in sinkage condition 10 $[\mathrm{mm}]$. This is representative result in the three trials

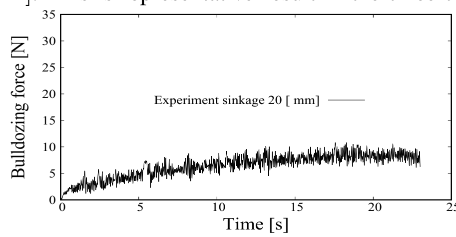

(b) Time history of the bulldozing force in sinkage condition 20 $[\mathrm{mm}]$. This is representative result in the three trials

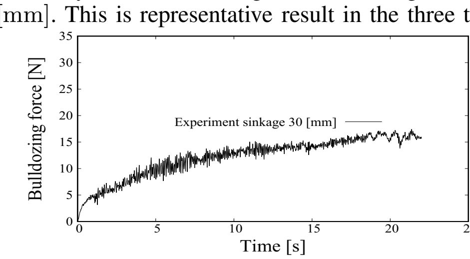

(c) Time history of the bulldozing force in sinkage condition 30 $[\mathrm{mm}]$. This is representative result in the three trials

Fig. 9: Experimental results of the bulldozing force in each sinkage.

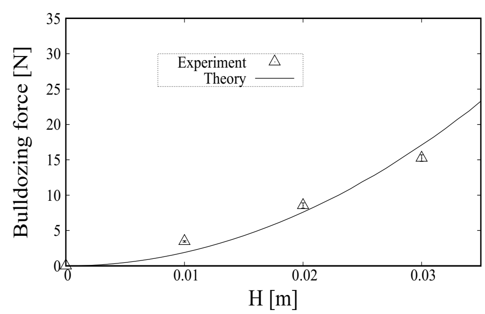

Fig. 10: Experimental and simulation results of bulldozing force (plate). The bars show standard deviation.

The difference of the force value in each wheel size is 0.07 $[\mathrm{N}]$ (sinkage 10 $[\mathrm{mm}]$), 0.33 $[\mathrm{N}]$ (sinkage 20 $[\mathrm{mm}]$) and 1.45 $[\mathrm{N}]$(sinkage 30 $[\mathrm{mm}]$), respectively. Therefore, the differences are relatively small. These results confirm that dependence on a wheel diameter to the bulldozing force is small on Silica sand No. 5.

V. CONCLUSIONS

In this paper, in order to confirm a bearing force of a backward wheel as bulldozing force, a bearing force generating mechanism was discussed. Then, the bulldozing force was calculated by the Hegedus's model and measured by the bulldozing experiment.

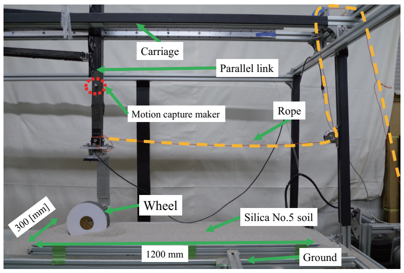

Fig. 11: Overview of experimental setting for wheel bulldozing test.

TABLE IV: Experimental settings for bulldozing wheel test.

Slope angle [°]	0
Sinkage [mm]	0, 10, 20, 30
Translational speed [mm/s]	36.5
Soil	Silica sand No. 5
Wheel diameter [mm]	150, 170, 200
Wheel width [mm]	40

It is suggested that the Hegedus's model showed a good approximation that corresponds with the experimental results. Moreover, from experimental results, dependence on a wheel diameter to the bulldozing force was small. Therefore, it is suggested that Hegedus's model can apply arbitrary wheel size. Additionally, from the wheel bulldozing experiment, the bulldozing force increases depending on sinkage. Therefore, we confirm that a deeper sinkage of a wheel can generate large bearing force in inching locomotion.

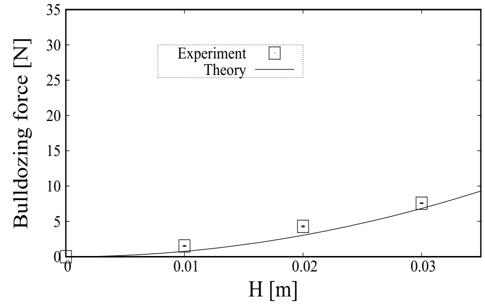

Fig. 12: Experimental and simulation results of bulldozing force (wheel). The bars show standard deviation.

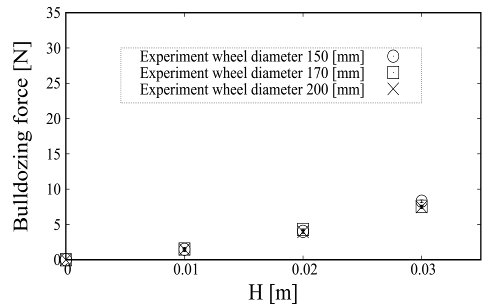

Fig. 13: Experimental results of bulldozing force in each wheel size. The bars shows standard deviation.

ACKNOWLEDGMENT

This work was supported by JKA and its promotion funds from KEIRIN RACE.

REFERENCES

[1] D. Ferguson, C. Kolecki, M. Siebert and D. Wilt, Evidence for Martain electrostatic charging and abrasive wheel wear from the Wheel Abrasion Experiment on the Pathfinder Sojourner rover, Journal of Geophysical research, Vol. 104, No. E4, pp. 8747-8789, 1999.

[2] R.E. Arvidson, S.W. Squyres and R.C. Anderson et al. Overview of the Spirit Mars Exploration Rover Mission to Gusev Crater: Landing site to Backstay Rock in the Columbia Hills, JOURNAL OF GEOPHYSICAL RESEARCH, Vol. 111, No. E02S01, 2006.

[3] A.S. McEwen, C.M. Dundas and S.S Mattson et al. Recurring slope lineae in equatorial regions of Mars, Nature Geoscience Vol. 7, pp. 53-58, 2004.

[4] A. Ellery, Planetary Rovers Robotic Exploration of the Solar System, Springer Praxis Books 2016.

[5] B.H. Wilcox, T, Litwin, and J. Biesiadecki et al. ATHLETE: A Cargo Handling and Manipulation Robot for the Moon, Jounal of Filed of Robotics, Vol. 24, No. 5, pp. 421-434, 2007.

[6] P.K. Soni and S. K. Singh, A Review: ATHLETE-ALL Terrain Hex-Limbed Extra-Terrestrial Explorer, International Journal of Advanced Engineering and Rsearch Development, Vol. 4, No. 4, pp. 410-416, 2017.

[7] S. Moreland, K. Skonieczny and D. Wettergreen, Inching Locomotion for Planetary Rover Mobility, IEEE Aerospace Conference 2011.

[8] K. Skonieczny, S.J. Moreland and V.W. Asnani et al. Visualizing and Analyzing Machine-soil Interactions using Computer Vision, Jounal of Filed of Robotics, Vol. 31, No. 5, pp. 820-836, 2014.

[9] C. Creager, K. Johnson and M. Plant et al. Push pull locomotion for vehicle extrication, Journal of Terramechanics, Vol. 57, pp. 71-80, 2015.

[10] N. Patel, R. Slage and R. Clemmet, The ExoMars rover locomotion subsystem, Journal of Terramechanics, Vol. 47, No. 4, pp. 227-242, 2010.

[11] R. Bauer, W. Leung and T. Barfoot, Development of a Dynamic Simulation Tool For the Exomars Rover, Proc. of The 8th International Symposium on Artifical Intelligence, Robotics and Automation in Space - iSAIRAS, Munich, Germany. 5-8 September 2005, (ESA SP-603, August 2005).

[12] A. Kermurdjian, V. Gromov and V. Mishkinyuk et al. Small Marsokhod Configuration. Proceedings of the 1992 IEEE International Conference on Robotics and Automation 1992.

[13] N. Ito, Discussions on the Slip-Sinkage of Tractor Drive Wheel (VI) -Transient Phenomenon at 100% Slippage-, Journal of the Japanese Society of Agricultural Machinery Vol. 36, No. 4, pp. 505-512, 1975.

[14] D. Fujiwara, K. Iizuka and D. Asami et al. Study on Traveling Performance for Variable, Wheel-Base Robot Using Subsidence Effect, International Journal of Electrical and Electronic Engineering & Telecommunications in press, 2018.

[15] J.Y. Wong, Theory of Ground Vehicles, John Wiley and Sons, 1978.

[16] J.Y. Wong and A.R. Reece, Prediction of rigid wheel performance based pn the analysis of soil-wheel streses: Part I. performance of driven rigid whees, Journal of Terramechanics, Vol. 4, No. 1, pp. 81-98, 1967.

[17] M.G. Bekker, Off-The-Road Locomotion, The University of Michigan Press, Ann Arbor, MI, USA, 1960.

[18] M.G. Bekker, Intoroduction to terrain-vehicle systems, The University of Michigan Press, Ann Arbor, MI, 1969.

[19] T. Shirai and G. Ishigami, Development of in-wheel sensor system for accurate measurement of wheel terrain interaction characteristics, Journal of Terramechanics, Vol. 62, pp. 51-61, 2015.

[20] E. Hegedus, A simplified method for the determination of bulldozing resistance. Land Locomotion Research Laboratory, Army Tank Automotive Command Report, 61, 1960.

[21] M. Kikumoto, S. Nichimura and K. Hayano, Soil Mechanics, Gakugei Shuppan Sha, p. 94, 2015 (in Japanese).

[22] S. Kozoe, T. Kasai and K. Kaneko et al. Relationship between mechanical properties and fiber mixture ratio in fiber-reinforced sand, Geosynthetics Engineering Journal, Vol. 27, pp. 127-132, 2012 (in Japanese).